

A System for Traded Control Teleoperation of Manipulation Tasks using Intent Prediction from Hand Gestures

Yoojin Oh¹, Tim Schäfer¹, Benedikt Rüter¹, Marc Toussaint^{2,3} and Jim Mainprice^{1,2}

¹Machine Learning and Robotics Lab, IPVS, University of Stuttgart, Germany

²Max Planck Institute for Intelligent Systems ; MPI-IS ; Tübingen/Stuttgart, Germany

³Technische Universität Berlin ; TUB ; Germany

Abstract—This paper presents a teleoperation system that includes robot perception and intent prediction from hand gestures. The perception module identifies the objects present in the robot workspace and the intent prediction module which object the user likely wants to grasp. This architecture allows the approach to rely on traded control instead of direct control: we use hand gestures to specify the goal objects for a sequential manipulation task, the robot then autonomously generates a grasping or a retrieving motion using trajectory optimization. The perception module relies on the model-based tracker to precisely track the 6D pose of the objects and makes use of a state of the art learning-based object detection and segmentation method, to initialize the tracker by automatically detecting objects in the scene. Goal objects are identified from user hand gestures using a trained a multi-layer perceptron classifier. After presenting all the components of the system and their empirical evaluation, we present experimental results comparing our pipeline to a direct traded control approach (i.e., one that does not use prediction) which shows that using intent prediction allows to bring down the overall task execution time.

I. INTRODUCTION

Intelligent robots can substitute or assist humans to accomplish complicated and laborious tasks. They are becoming present in our lives from production lines to hospitals and our homes. However, many applications remain challenging for robots to function in full autonomy. Teleoperation is an intermediate solution for controlling robots in scenarios where the task objectives have to be decided in real-time, such as disaster relief [1], autonomous driving [2], or assistive devices [3,4].

Shared control has been investigated to effectively blend user and autonomous control during teleoperation. The linear blending paradigm introduced by Dragan et. al [5] is still widely applied in many shared control frameworks [4,6,7]. In the approach, the amount of arbitration is dependent on the confidence of user prediction. However, the user loses control authority when the robot predicts the user’s intent with high confidence.

Some works allocate maximum control authority to the user by providing minimal assistance only when it is necessary. Broad et. al. [8] introduced minimum intervention shared control that computes whether the control signal leads to an unsafe state and replaces the user control if so. Our recent work [9] formulates shared control as an optimization problem, which can conveniently balance control authority and optimality when a complete robot policy is available.

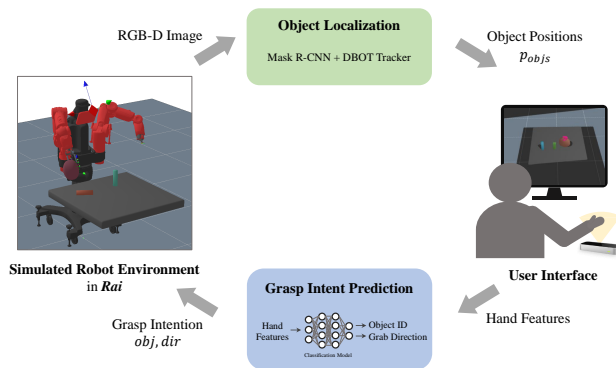


Fig. 1: Overview of the teleoperation system

While these works are relevant to the teleoperation of simple manipulation task where direct control is not optimal, they are generally limited to controlling the end-effector of the robot by blending between direct and autonomous control. They rely on a semantic mapping of the workspace but they do not let the autonomy take complete advantage of these models, so as to maximize control authority. Additionally when using interfaces such as hand gestures controllers, direct teleoperation is often nearly impossible as the mismatch between the kinematics of the robot and hand gestures is too large to produce fluid movements.

Hence in this systems paper, we demonstrate a complete *traded control* teleoperation implementation, where the user specifies the task objectives and executes the motion autonomously. Contrarily to the aforementioned approaches, it does not blend between direct and autonomous control. Our system makes use of available models, in terms of object poses and shapes to plan robot motion trajectories.

We present and evaluate all components needed for such a system, which can be decomposed into three parts: 1) a perception pipeline capable of identifying and tracking objects, 2) an intent estimation system that can identify which objects to grab and how, 3) a motion planning system that can produce accurate manipulation motion in accordance to the human intent. *

After presenting the individual components, we assess the accuracy of the the different modules on dedicated tasks. We evaluate the object localization and tracking module

*Video available at <https://sites.google.com/view/ohyn-teleoperation-pipeline/home>

on several objects in simulation, test the accuracy of our grasp intent prediction module using a dataset of trajectories. Finally, we present results using our grasp intent inference module, where various users are simulated using degraded user trajectories collected using the hand gesture controller.

We summarize our main contributions as the following:

- A teleoperation system capable of traded control using hand gestures
- Simulated user experiment assessing the capacity of our grasp intent prediction module to perform teleoperation of pick and place motions
- A solution for automatic initialization of an existing object tracking module using Mask R-CNN [10]

This paper is structured as follows: we present related work in Section II.

Section III presents our user interface. Section IV presents our object tracking pipeline, including the combination of Mask R-CNN and a model-based object tracker. Section V presents the assessment of the modules in our pipeline. Conclusions are drawn in Section VI.

II. BACKGROUND AND RELATED WORK

A. Traded Control in Teleoperation

Traded control is a discrete switching mechanism between high-level robot autonomy and low-level control depending on predefined circumstances. It is also referred to as *control switching*, as the system allocates all-or-none assistance rather than a blended spectrum between user and robot controls. The operator initiates a sub-task or behavior for the robot and the robot performs the sub-task autonomously while the operator monitors the robot [1,11]. [12] showed that intent-based traded control can improve teleoperation performance and alleviate difficulties in high-latency teleoperation scenarios.

B. Hand Gesture Recognition for Robot Control

The Leap Motion controller (Ultra Leap, <https://www.ultraleap.com/>) is a consumer-grade, markerless motion capture sensor that tracks hand gestures and finger movements up to 200 Hz. [13] showed that its accuracy is below 2.5mm, however, the controller shows inconsistent performance due to its limited sensory range [14]. Nevertheless, its simplicity and its capability to track the hand in 6-Dof are the reasons for its application.

Prior works used deep learning to improve the accuracy of the gesture recognition, such as SVMs and random forests [15], or neural networks using radial basis functions (RBF) [16]. Similar to [17], we propose to train a gesture classifier (i.e., which object is intended) for hand motion recognition rather than mapping hand features directly to robot configurations. Achieving higher accuracy is easier on classification than regression (i.e., predicting accurate positions) tasks, which is one of the justifications for our traded control approach.

C. Depth Based Object Tracking (DBOT)

We utilize the implementation of depth-based object tracking methods described in [18] (“particle tracker”) and [19] (“Gaussian tracker”) to acquire the 6D pose of objects during teleoperation. Compared to recent learning-based methods such as PoseCNN [20] and DenseFusion [21], the methods take a model-based approach.

The particle tracker in DBOT tracks objects by computing a posterior distribution over the object using a dynamic Bayesian network for inference [18], while the Gaussian tracker improves the performance of a Gaussian filter using a robustification method as well as reducing the filter’s computational complexity [19]. This approach has the advantage of being robust without requiring any extra tuning or pre-training.

III. TELEOPERATION USING TRADED CONTROL

A. Hand Gesture Based Robot Control

The user provides grasping intentions and commands by performing reach-and-grasp motions with the right hand as if the user naturally reaches and grasps an object while looking at the environment from the robot’s perspective.

The hand motion is captured using a Leap Motion controller. Features are captured and published via ROS topics at a frame rate of 180Hz. Since the user is actually reaching towards an invisible object, the grabbing positions vary significantly as shown in 2a. We resolve this issue with a traded control paradigm and learning a classifier to distinguish how the user is intending to grab the object.

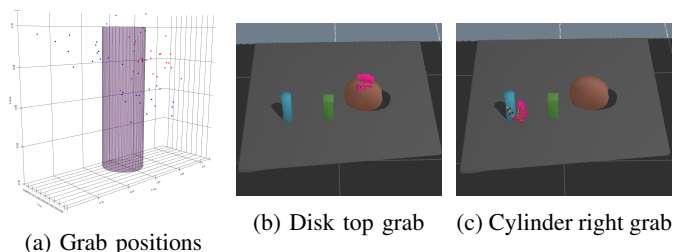


Fig. 2: (a) Grab positions from users tracked with the Leap Motion controller, top grab (red)/right grab (blue). (b), (c) User interface for reach and grab motion in a setting with three objects.

B. Traded Control

To alleviate the inconsistent hand tracking performance, we adopt a traded control method rather than a continuous shared control paradigm. This also relieves the problems that arise from the physical difference between the human arm and the robot arm.

Once objects are identified as described in Section IV, we predict the user’s intent of the target object and in which direction the user is intending to grasp. As soon as the intention is identified, the robot controller executes the object reach and grab motion. The user still maintains control authority by having the ability to decide in which order to grab the set of objects, that is, we rely on the human user

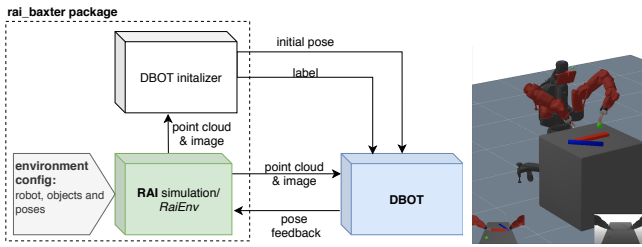


Fig. 3: Overview of the object tracking pipeline and an image of the simulated robot environment.

for high-level decision making and the robot takes care of the low-level control and motion planning.

C. Grasp Intention Prediction

We train a multi-layer perceptron using supervised learning to classify the goal object and the grasp direction. We assume a fixed set of objects ($m=3$) along with their positions and two possible grab directions (top/right, $n=2$), as shown in Figures 2b and 2c.

The input includes eight features: distances from the hand objects, x-component of the hand position, x-component of the hand direction, x,y-components of the palm normal vector, and y-rotation of the hand are selected through experience. The model consists of three dense layers of 64 hidden units that are connected to two separate layers of two units and outputs the class labels.

IV. OBJECT TRACKING PIPELINE

The object tracking pipeline is automatically initialized and tracks the 6D pose of rigid objects. We make use of the existing object tracking library [18,19] and provide a solution to alleviate the burden of manual initialization. The pipeline consists of two modules: object tracker initializer (DBOT initializer) and the object tracker (DBOT) as shown in Figure 3. The DBOT initializer receives camera images of the environment (see Figure 4) and predicts the initial pose as well as the semantic label of observed objects.

A. Automated Object Tracker Initialization

DBOT assumes that the initial pose of the object is given. In practice, this initialization is done by the user by manually positioning a marker over the object’s depth image in a 3D visualization of the depth image. We use Mask R-CNN [10], a state of the art instance segmentation method, to automate the initialization process by identifying the masks and the labels using transfer learning.

Once the depth pixels are segmented from the depth image using the object mask, we use point cloud registration to compute the object’s 6D pose. Utilizing the labels from the Mask R-CNN, the corresponding mesh model of the object is loaded and a set of points are sampled from the mesh as a reference point cloud for registration. Rigid registration is performed using the coherent-point-drift (CPD) algorithm [22], and we use the average position of the masked point cloud as a rough initialization during the registration. The output of the CPD is a 4×4 homogeneous

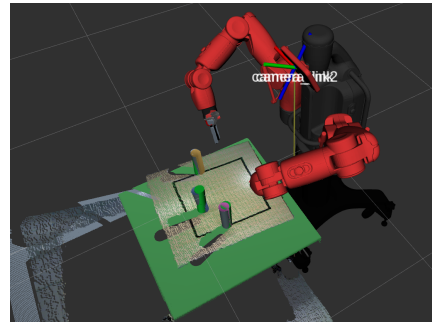


Fig. 4: Snapshot of our object tracking with real images

transformation matrix. We refer to this estimated pose as *mesh_pose*.

The process takes approximately 1-16 seconds, depending on the number of tracked objects and the number of iterations during point cloud registration. The step is performed once to initialize the DBOT tracker.

B. DBOT Tracker

Once the DBOT trackers are successfully initialized, the simulation or a real robot system can subscribe to the refined poses from DBOT and use the information to perform precise object manipulation. The DBOT tracker runs with 10Hz for up to 7 objects on CPU. The performance can be further improved by utilizing GPU.

V. EXPERIMENTS

A. Simulated Robot Environment

The environment consists of the Baxter robot with graspable objects on a table as shown in Figure 3 right. A virtual depth camera is added on Baxter’s head display to generate first-person view images (RGB-D).

The simulated environment is created using the *RAI*[†] interface. RAI includes a physics-simulated environment as well as a robot motion optimization solver for k-Order Motion Optimization (KOMO) problem[23]. The interface provides simple functionality to define motion optimization problems, by specifying the list of optimization objectives that represent cost terms or in-/equality constraints.

B. Mask R-CNN Transfer Learning on a Synthetic Dataset

We use transfer learning to tune the Mask R-CNN to ensure the detection of custom objects. We collect images of the simulated robot environment including the following objects: a cube, a sphere, a toy, a teapot, a cup, a jug, and a bowl, as shown in Figure 6.

The simulated images are not like real images as they do not include noise, shadows, irregular lighting conditions, or texture. The images are augmented during training to ensure the network generalizes towards real or non-perfect images. Augmentations include flipping the image, affine transformation, light contrast, blur/sharpen, and color modifications. The dataset is also collected with arbitrary robot arm joint positions included in the image so that Mask R-CNN learns to neglect robot arms during detection.

[†]<https://github.com/MarcToussaint/rai>

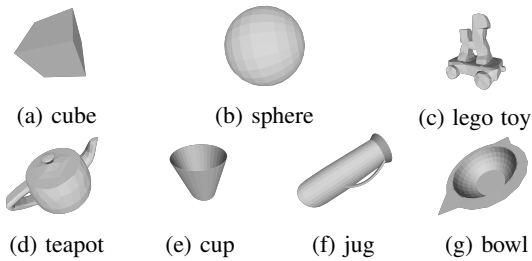


Fig. 6: Objects used to train Mask R-CNN

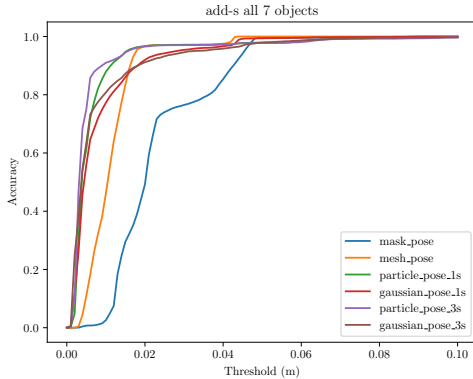


Fig. 7: Accuracy-threshold curve of the average ADD-S for seven objects with maximum threshold of 10cm.

We obtained detection rates from the Mask R-CNN ranging from 92% to 95% with an error rate between 0.16% to 0.74% based on different training settings such as the number of epochs (10 to 80 epochs) and the dataset size (107 to 50K samples). The detection rate is defined as the number of classified objects with respect to the number of ground truth objects. The error rate is defined as the number of wrong class predictions with respect to the number of classified objects. The rest consists of undetected objects, presumably simply not detected, out of sight, or just partially visible. We do not report detailed results for each setting, as its effect turned out to be marginal when comparing the results of the whole initialization pipeline. As long as the detected label is correct, a decent mask is adequate for estimating the initial pose described in Section IV-A.

The model used during the evaluation of the pose initialization shown in Table I was trained with unmodified images with 40 epochs. The detection rate of the Mask R-CNN was 92.73% with an error rate of 0.16% out of a set of 4,798 random samples. The images of the samples were not included during the Mask R-CNN training and did not contain the arms of the Baxter robot.

C. Accuracy of the Initial Object Pose Estimation

We evaluate the accuracy of the pose estimation using the metric proposed in [20]. The average distance is computed using the closest point distance of the pairwise distances between two 3D models with ground truth transformation (translation t , rotation R) and estimated transformation

	mask		mesh		particle 1s		gaussian 1s		particle 3s		gaussian 3s	
	t	R	t	R	t	R	t	R	t	R	t	R
cube	89.1	90.3	96.0	97.4	97.0	93.9	97.0	97.7	97.2	90.7	96.9	
sphere	76.1	79.2	97.0	97.9	97.0	97.5	97.0	97.9	97.0	98.0	97.0	
lego_toy	66.7	80.2	90.2	85.0	92.2	84.8	92.3	84.9	92.4	83.0	92.3	
teapot	77.8	80.0	90.7	91.7	93.3	86.5	92.8	94.0	95.2	91.2	94.8	
cup	90.9	90.2	95.0	94.0	95.9	85.1	95.6	94.3	96.2	77.1	95.7	
jug	69.8	77.3	90.2	93.6	92.4	74.8	92.8	95.1	95.3	89.9	96.2	
bowl	69.3	70.4	84.4	81.0	87.7	86.6	84.9	81.1	88.7	80.8	85.6	
MEAN	77.1	81.1	91.9	91.5	93.7	87.0	93.2	92.1	94.6	87.2	94.1	

	mesh		particle 1s		gaussian 1s		particle 3s		gaussian 3s	
	AUC	<2cm	AUC	<2cm	AUC	<2cm	AUC	<2cm	AUC	<2cm
cube	93.8	100.0	96.8	100.0	95.6	99.7	97.0	100.0	94.3	98.8
sphere	88.6	100.0	96.1	100.0	96.0	100.0	96.1	100.0	96.1	100.0
lego_toy	90.8	99.3	93.3	98.1	93.4	96.7	93.4	97.3	92.3	88.4
teapot	88.2	100.0	93.7	100.0	91.3	94.0	95.2	100.0	93.8	95.2
cup	92.9	100.0	95.1	99.0	92.0	92.7	95.3	98.9	87.8	86.4
jug	84.6	98.8	91.8	99.6	86.6	82.7	95.2	99.6	93.3	94.5
bowl	80.4	78.7	83.6	80.2	85.5	78.1	82.9	80.2	83.9	75.0
MEAN	88.5	96.7	92.9	96.7	91.5	92.0	93.6	96.6	91.6	91.2

TABLE I: Accuracy object tracking pipeline. The upper table shows position and orientation individually. The lower table shows the area under the ADD-S curve (AUC) and <2cm metric.

(translation \hat{t} , rotation \hat{R}):

$$\text{ADD-S} = \frac{1}{m} \sum_{x_1 \in \mathcal{M}} \min_{x_2 \in \mathcal{M}} \|(Rx_1 + t) - (\hat{R}x_2 + \hat{t})\| \quad (1)$$

in a set \mathcal{M} with m number of points, for both symmetric and asymmetric objects. Following prior works [20,21], we report the area under the ADD-S curve (AUC) with a threshold up to 0.1m by computing the pose accuracy while increasing the threshold. Similarly, we also measure the percentage of ADD-S below a threshold of 2cm, which is the minimum tolerance for robot grasping manipulation.

Figure 7 and Table I show the accuracy of different object tracking methods including the method described in Section IV-A. The *mask_pose* (or *mask* in Table I) indicates the center position of the masked point cloud with an offset (2cm in the z-axis of the camera coordinates) added to compensate the bias in the point cloud. The *mask_pose* does not include rotation which explains the low AUC, but is a good baseline when comparing translation. The *mesh_pose* shows better precision in translation compared to the *mask_pose*, nonetheless, its main role is to provide an initial rotation estimation to initialize DBOT.

D. Accuracy of the DBOT Tracker

We report the result of the estimated pose once the DBOT tracker is tracking the object after receiving the initial *mesh_pose*. The object pose from the DBOT is captured after 1 second and 3 seconds after initialization while the object is kept static. Table I shows that both trackers outperform the initial *mesh_pose*. This indicates that the tracker was able to

refine the pose towards the correct object pose after receiving the estimated pose.

The particle tracker refined the pose faster and is more accurate than the Gaussian tracker. An assumption is that the Gaussian tracker is less robust to inaccurate initialization. The authors of DBOT mentioned in their paper [19] that the particle tracker is slightly more robust, but the Gaussian tracker is more precise. The Gaussian tracker can tolerate distortions in the input point cloud as well as occluded settings where the particle tracker is not able to track.

We compare our objects to similar objects in the YCB dataset in terms of size and form, as shown in Table II. A direct comparison of the results to prior work in pose detection [20,21] is not completely fair, due to the different datasets used for evaluation and that we utilized simulated images. However, it justifies the feasibility of our approach and its applicability in robot manipulation.

	PoseCNN [20]		DenseFusion [21]		Own results				
	AUC <2cm	AUC <2cm	AUC <2cm	own class	mesh AUC <2cm	particle 3s AUC <2cm	jug	pitcher base	
pitcher base	97.8	100.0	97.1	100.0	jug	84.6	98.8	95.2	99.6
bowl	81.0	54.9	88.2	98.8	bowl	80.4	78.7	82.9	80.2
mug	95.0	99.8	97.1	100.0	cup	92.9	100.0	95.3	98.9
wood block	87.6	80.2	89.7	94.6	cube	93.8	100.0	97.0	100.0
MEAN	90.35	83.73	93.03	98.35		87.93	94.38	92.6	94.68

TABLE II: Evaluation of 6D pose (ADD-S) on YCB-Video dataset.

The mean AUC of DenseFusion for the four objects is 93.03%. The mean AUC of the *mesh_pose* is 87.93% and for the particle tracker after 3s is 92.6%. As already mentioned, the direct comparison is not totally fair, but as an interpretation that the object tracking pipeline is robust enough to be applicable in a robot manipulation setting.

E. Accuracy of the Grasp Intent Prediction

We collected reach-and-grab motion trajectories from two users (1 male, 1 female). Each trajectory consisted of around 2~5 seconds and we collected a total of 350 trajectories for training in four different environment settings. The users started with their right hand above the Leap Motion controller and reached forward to grab a target object in a specific direction (right or top) while looking at the display similar to Figures 2b and 2c. The start and termination of the trajectories were defined by a key press.

Figure 8 shows the average prediction accuracy over 18 grasp episodes of one environment using trajectories excluded during training. The overall prediction accuracies are 79.4% and 77.4% for target object prediction and grab direction prediction. The goal object prediction accuracy reached 100% before reaching 70% of the episode duration, and the average accuracy for predicting the direction reached up to 89% at termination. The low accuracy during the first 20% of the episode resulted from the time gap between the start of recording and the start of the movement.

The reader may note that the prediction results are not optimal and optimization of the hyperparameters can be

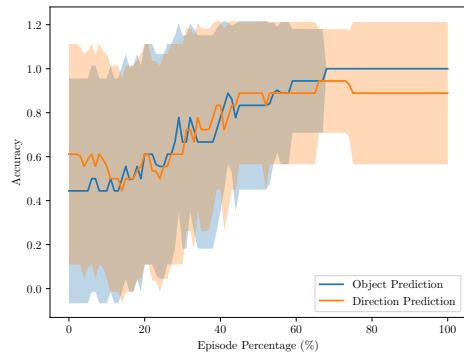


Fig. 8: Prediction accuracy of the grasp intention prediction averaged over the duration of the episode

carried out for better results. Utilization of recurrent neural networks may also help with improving the early prediction accuracy.

F. Teleoperation Task Experiment Setup

We designed a teleoperation task for manipulation to test the efficacy of the system. We hypothesize that the earlier the goal object is identified, the earlier the robot can start planning the motion, which would lead to faster task execution in a traded control setting.

We carried out a simulated user study by simulating different behaviors of users. We collected trajectories from three different types of virtual users

- *Normal* user consists of trajectories collected from human users
- *Noisy* user by injecting a Gaussian noise to the *Normal* user at each time step
- *Biased* random offset over the *Normal* user trajectory to simulate imperfect perception during teleoperation, e.g., recognizing the object as closer than it actually is.

The difference between a *Noisy* user and a *Biased* user is that the *Biased* user has the same random noise over the trajectory whereas the noise in the *Noisy* user changes every time step.

The task is to perform a sequence of picking motions, to grab three objects from a table. The user decides which object to grab and demonstrates the picking motion.

We assume that the poses of all objects are known by fusing the framework presented in Section IV, but the robot must infer in which order the objects are grabbed. A goal object is identified when the robot predicts the same target for t consecutive time steps ($t=80$). The prediction of the first k time steps are neglected to reduce the prediction error in the beginning of the episode ($k=300$).

G. Evaluation of Control Modes

We denote *Early* mode as the control mode in which the robot starts to plan its grasping trajectory towards the predicted object during user demonstration. We compare this mode with *Late* mode, where the robot does not start motion planning until the user finishes the demonstration.

Criteria	Control Mode	User Mode			MEAN
		Normal	Noisy	Biased	
Time until Execution (s)	Early	9.6±1.1	10.3 ± 0.9	10.1± 1.3	10.
	Late	14.6± 1.4	14.7 ± 1.2	14.1 ± 1.5	14.5
Episode Duration (s)	Early	33.1 ±5.6	32.5 ± 3.7	33.9±5.3	33.2
	Late	38.6 ±5.1	39.2 ± 3.1	38.1±5.4	38.6
Object Prediction (%)	Early	0.86± 0.49	0.89 ± 0.47	0.89 ± 0.62	0.88
	Late	0.97± 0.28	0.97 ± 0.28	0.89 ± 0.62	0.94
Direction Prediction (%)	Early	0.94± 0.37	0.97 ± 0.28	0.89 ± 0.62	0.93
	Late	1± 0	0.97 ± 0.28	0.97 ± 0.28	0.98

TABLE III: Teleoperation results for different simulated users and control modes

The system was evaluated according to the following criteria: time taken to predict goal object (time until execution), episode duration, prediction accuracy (goal prediction, direction prediction) when the robot identified the goal. Table III shows the results averaged over 12 episodes. The time until execution is summed up over three object grasps and the episode duration indicates the total time for picking three objects including robot motion planning time. Although it shows a compromise in the prediction accuracy, early motion planning and execution based on goal prediction resulted in shorter episode duration, as hypothesized. It is shown that it was approx. 5 seconds faster than when the robot started motion planning once the user finished the trajectory.

The *Noisy* user and the *Biased* error took longer before the robot confidently identified the goal. However, there was no penalty in the prediction accuracy except in the direction prediction for the *Biased* user in *Early* mode. The prediction model was robust enough to tolerate the noisy settings. Overall, the results show that the proposed traded control system can improve teleoperation performance while using noisy hand gestures to control the robot.

VI. CONCLUSIONS

We presented a teleoperation system that utilizes intuitive human grabbing hand gestures to perform sequential manipulation tasks. To mitigate the issues that arise when using hand gestures, the robot autonomously generates a grasping or retrieving motion using trajectory optimization as soon as the robot identifies the user’s intention.

For the object tracking pipeline, we proposed the combination of Mask R-CNN [10] and the model-based object tracker DBOT [19] for automatic initialization and object localization. In addition, we trained a prediction model to identify the user intent from grabbing hand gestures during traded control so that the robot can start planning its trajectory in advance. The simulated user study indicated that using intent prediction brought down the overall task execution time.

As the majority of our work is done in a simulated environment, limitations may arise during the application of the system in a real robot setting. We will focus on the application of the system in a real robot setting for future work.

ACKNOWLEDGMENT

This work is partially funded by the research alliance “System Mensch”. The authors thank the International Max Planck Research School for Intelligent Systems (IMPRS-IS) for supporting Yoojin Oh.

REFERENCES

- [1] C. Phillips-Grafflin, *et al.*, “From autonomy to cooperative traded control of humanoid manipulation tasks with unreliable communication,” *Journal of Intelligent & Robotic Systems*, vol. 82, no. 3-4, 2016.
- [2] M. Johns, *et al.*, “Exploring shared control in automated driving,” *ACM/IEEE Int. Conf. on Human-Robot Interaction (HRI)*, 2016.
- [3] K. Muelling, *et al.*, “Autonomy infused teleoperation with application to brain computer interface controlled manipulation,” *Autonomous Robots*, vol. 41, no. 6, 2017.
- [4] A. Goil, *et al.*, “Using machine learning to blend human and robot controls for assisted wheelchair navigation,” in *IEEE 13th International Conference on Rehabilitation Robotics (ICORR)*, 2013.
- [5] A. D. Dragan and S. S. Srinivasa, “A policy-blending formalism for shared control,” *The International Journal of Robotics Research*, vol. 32, no. 7, 2013.
- [6] S. J. Anderson, *et al.*, “Experimental performance analysis of a homotopy-based shared autonomy framework,” *IEEE Transactions on Human-Machine Systems*, vol. 44, no. 2, 2014.
- [7] M. Gao, *et al.*, “Contextual task-aware shared autonomy for assistive mobile robot teleoperation,” *IEEE/RSJ Int. Conf. on Intel. Robots And Systems (IROS)*, 2014.
- [8] A. Broad, *et al.*, “Operation and imitation under safety-aware shared control,” in *Workshop on the Algorithmic Foundations of Robotics*, 2018.
- [9] Y. Oh, *et al.*, “Natural gradient shared control,” *IEEE Int. Symp. on Robot and Human Interactive Communication (RO-MAN)*, 2020.
- [10] K. He, *et al.*, “Mask r-cnn,” *IEEE Int. Conf. on Computer Vision (ICCV)*, 2017.
- [11] J. Kofman, *et al.*, “Teleoperation of a robot manipulator using a vision-based human-robot interface,” *IEEE transactions on industrial electronics*, vol. 52, no. 5, 2005.
- [12] J. Bohren and L. L. Whitcomb, “A preliminary study of an intent-recognition-based traded control architecture for high latency telemanipulation,” *IEEE/RSJ Int. Conf. on Intel. Robots And Systems (IROS)*, 2017.
- [13] F. Weichert, *et al.*, “Analysis of the accuracy and robustness of the leap motion controller,” *Sensors*, vol. 13, no. 5, 2013.
- [14] J. Guna, *et al.*, “An analysis of the precision and reliability of the leap motion sensor and its suitability for static and dynamic tracking,” *Sensors*, vol. 14, no. 2, 2014.
- [15] G. Marin, *et al.*, “Hand gesture recognition with jointly calibrated leap motion and depth sensor,” *Multimedia Tools and Applications*, vol. 75, no. 22, 2016.
- [16] W. Zeng, *et al.*, “Hand gesture recognition using leap motion via deterministic learning,” *Multimedia Tools and Applications*, vol. 77, no. 21, 2018.
- [17] W. Qi, *et al.*, “Multi-sensor guided hand gestures recognition for teleoperated robot using recurrent neural network,” *IEEE Robotics and Automation Letters*, 2021.
- [18] M. Wüthrich, *et al.*, “Probabilistic object tracking using a range camera,” *IEEE/RSJ Int. Conf. on Intel. Robots And Systems (IROS)*, 2013.
- [19] J. Issac, *et al.*, “Depth-based object tracking using a robust gaussian filter,” *IEEE Int. Conf. Robotics And Automation (ICRA)*, 2016.
- [20] Y. Xiang, *et al.*, “Posecnn: A convolutional neural network for 6d object pose estimation in cluttered scenes,” *arXiv preprint arXiv:1711.00199*, 2017.
- [21] C. Wang, *et al.*, “Densefusion: 6d object pose estimation by iterative dense fusion,” *IEEE Conf. on Computer Vision and Pattern Recognition (CVPR)*, 2019.
- [22] Kenta-Tanaka *et al.*, “probreg.” [Online]. Available: <https://probreg.readthedocs.io/en/latest/>
- [23] M. Toussaint, “Komo: Newton methods for k-order markov constrained motion problems. e-print,” *arXiv preprint arXiv:1407.0414*, 2014.